Analysis of long-period seismic waves excited by the 2012 Off-Sumatra earthquake

Zacharie Duputel, Victor Tsai, Hiroo Kanamori, Luis Rivera, Lingsen Meng, Jean-Paul Ampuero, Joann Stock.

1. Abstract

Great strike-slip earthquakes are very uncommon and it is known that many of them involve remarkable rupture complexity. On 11 April 2012, the equatorial Indian Ocean was hit by a Mw=8.6 earthquake, followed two hours later by another Mw=8.2 event. Our analysis for the Mw=8.6 mainshock reveals a remarkable rupture complexity and indicates a large centroid depth (~30km). To resolve the rupture process, we developed a method to invert long period seismic data for multiple-point-source parameters. The optimum source model at long period consists of two sources with Mw=8.5 and Mw=8.3. To analyze the Mw=8.2 aftershock, we removed the perturbation due to surface-wave arrivals of the mainshock by subtracting the corresponding synthetics. Our results suggests that the Mw=8.2 aftershock had a large centroid depth between 30 km and 40 km. The large centroid depths observed for the mainshock and the Mw=8.2 aftershock suggest that this sequence most likely breaks the entire oceanic lithosphere thickness. This major earthquake sequence thus brings a new perspective to the seismotectonics of the equatorial Indian Ocean and reveals active deep lithospheric deformations that may ultimately lead to a localized plate boundary.

2. Methods

2.1 W-phase Inversion for Point-Source Geometry. Point-source parameters of Mw>=5.8 events during the 2012 Off-Sumatra earthquake sequence are inverted using the W phase algorithm (**Fig. 1**). The moment tensor components as well as the centroid locations and timings are resolved following the procedure described by Duputel et al. (2012).

2.2 Surface-wave directivity and radiation pattern. To obtain the surface-wave radiation patterns, seismograms $U(\omega,\Delta,\varphi)$ are equalized to Δ_0=90° (**insets in Fig. 2a-b**). To further analyze the directivity, we measure the ratio between observed amplitude and predicted surface-wave amplitudes for a point-source in the 200-400 s passband (**Fig. 2a-b**).

2.3 Surface-wave moment rate functions. We compute broadband (25s-600s) R1 Rayleigh-wave moment rate functions by deconvolving point-source synthetics from data (**Fig. 2c**). The deconvolution is performed using the projected Landweber method imposing causality and positivity. We use SEM synthetics for a 3D Earth model (S362ANI and Crust2.0).

2.4 Multiple point source analysis. To account for the MRFs suggesting at least two distinct subevents for the mainshock, we perform a two-point-source inversion (**Fig. 1** and **Fig. 3**). We invert for the subevent moment tensors, locations (latitudes, longitudes, depths), time delays and half durations using a modified version of the Neighborhood Algorithm sampler.

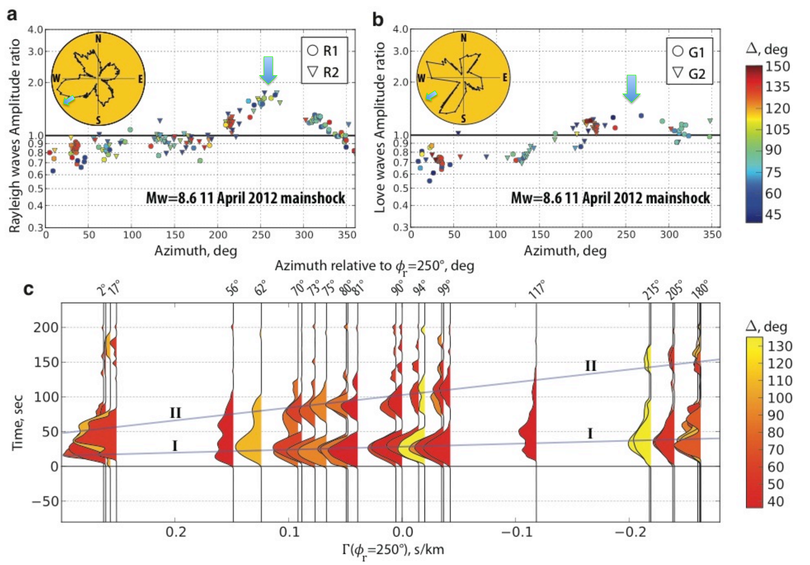

Figure 2. Long period Surface-wave analysis for the Mw=8.6 mainshock. Obs./Pred. ratios are presented for **a,** Rayleigh waves and **b,** Love waves. The Inset diagrams are equalized Rayleigh and Love waves. **c,** R1 Rayleigh wave Moment Rate Functions (MRFs) ordered as a function of the directivity parameter $\Gamma=\cos(\phi-\phi_r)/c$, assuming ϕ_r = 250° and c=3.8km/s. Amplitude ratios and R1 MRFs are colored as a function of the epicentral distance (Δ).

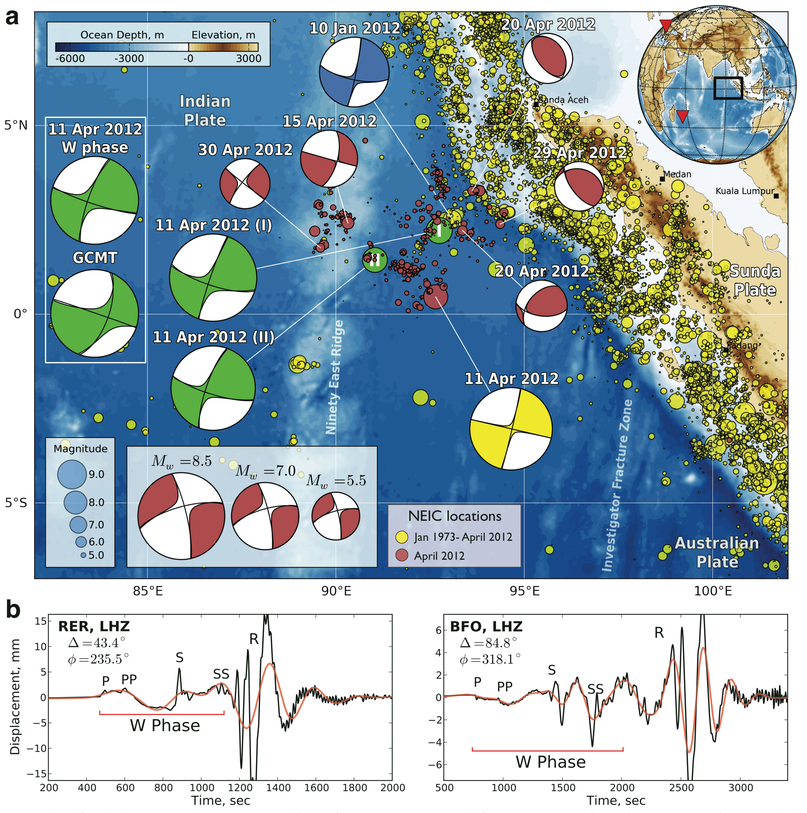

Figure 1. The 2012 Sumatra great earthquake sequence. **a,** Off-Sumatra earthquake region. The Mw=8.6 mainshock can be decomposed in two subevents (green mechanisms and circles labeled I and II). The W phase and Global CMT solutions for the mainshock (inset green mechanisms), the W phase solutions for the 10 January foreshock (blue mechanism), for the Mw=8.2 aftershock (yellow) and for the 5.8<=Mw<8.2 aftershocks (red) are shown. **b,** W phase waveforms recorded at station RER and BFO during the mainshock. The black trace is the broad-band data and the red trace is the data filtered in the 200-1000 s passband.

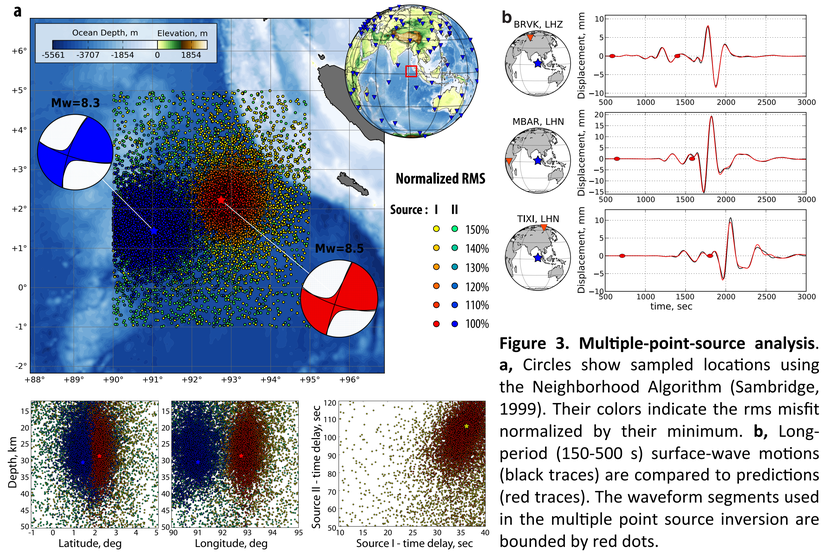

Figure 3. Multiple-point-source analysis. **a,** Circles show sampled locations using the Neighborhood Algorithm (Sambridge, 1999). Their colors indicate the rms misfit normalized by their minimum. **b,** Long-period (150-500 s) surface-wave motions (black traces) are compared to predictions (red traces). The waveform segments used in the multiple point source inversion are bounded by red dots.

3. First order directivity analysis

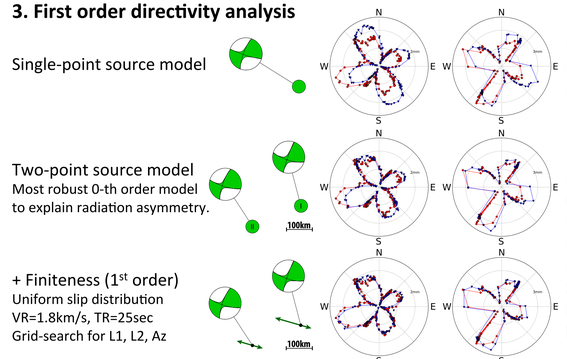

Figure 4: Comparison of observed and predicted surface-wave radiation patterns for three simple rupture models: Single-point source, Two-point source and two WNW-ESE bilateral ruptures with significant directivity in the WNW direction. Comparison of observed (red) and predicted (blue) equalized amplitudes for Rayleigh R1, R2 (left) and Love G1, G2 (right).

4. Comparison with preliminary finite-fault modeling

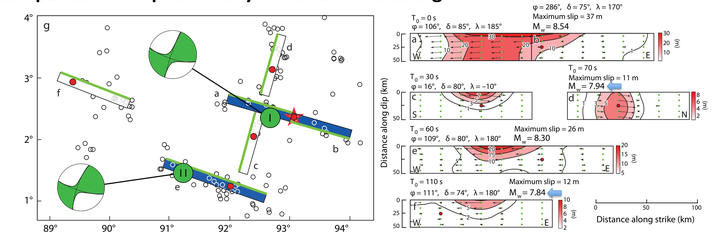

Figure 5. Comparison with the slip distribution model proposed by Yue et al. (2012). There is a dominant contribution from WNW-ESE faults, consistent with the first order directivity analysis.

5. Evidence of complete lithospheric failure

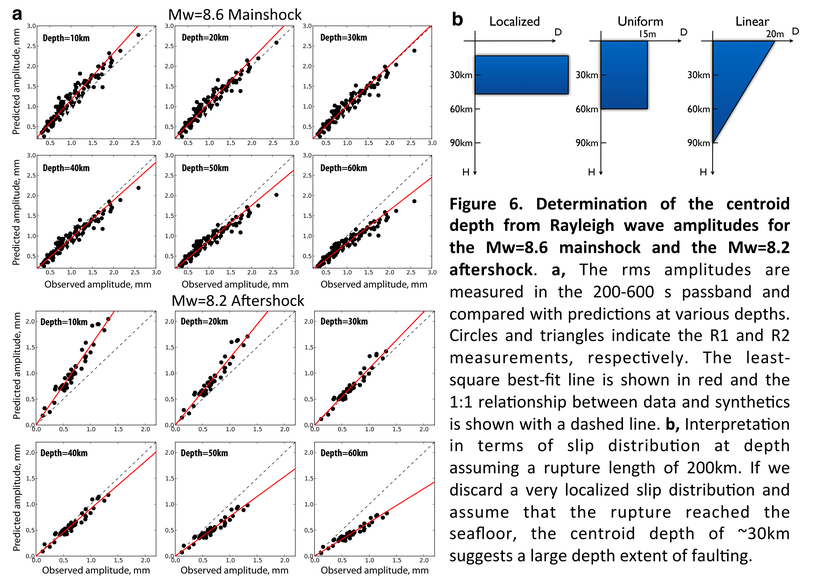

Figure 6. Determination of the centroid depth from Rayleigh wave amplitudes for the Mw=8.6 mainshock and the Mw=8.2 aftershock. **a,** The rms amplitudes are measured in the 200-600 s passband and compared with predictions at various depths. Circles and triangles indicate the R1 and R2 measurements, respectively. The least-square best-fit line is shown in red and the 1:1 relationship between data and synthetics is shown with a dashed line. **b,** Interpretation in terms of slip distribution at depth assuming a rupture length of 200km. If we discard a very localized slip distribution and assume that the rupture reached the seafloor, the centroid depth of ~30km suggests a large depth extent of faulting.

6. Summary

The Mw=8.6 Sumatra earthquake involved a remarkable rupture complexity. Our analysis of long period seismic waves yielded a simple two point source model and reveals substantial deep lithospheric deformation that may eventually lead to the formation of a localized plate boundary.

7. References

Duputel, Z., Kanamori, H., Tsai, V.C., Rivera, L., Meng, L., Ampuero, J.-P., Stock, J., 2012. Earth Planet Sci. Lett., 351, 247-257.
Duputel, Z., Rivera, L., Kanamori, H., Hayes, G., 2012. Geophys. J. Int. 189, 1125-1147.
Sambridge, M., 1999. Geophys. J. Int. 138, 479-494.
Yue, H., Lay, T., Koper, K.D., 2012. Nature. 490, 245-249.